EUKARYOTIC CELL, Apr. 2005, p. 775–786 Vol. 4, No. 4
1535-9778/05/$08.00+0 doi:10.1128/EC.4.4.775–786.2005

Intracellular Role of Adenylyl Cyclase in Regulation of Lateral Pseudopod Formation during *Dictyostelium* Chemotaxis

Vesna Stepanovic,[1] Deborah Wessels,[1] Karla Daniels,[1] William F. Loomis,[2] and David R. Soll[1]*

W. M. Keck Dynamic Image Analysis Facility, Department of Biological Sciences, The University of Iowa, Iowa City, Iowa,[1] and Department of Biology, University of California—San Diego, La Jolla, California[2]

Received 20 December 2004/Accepted 7 February 2005

Cyclic AMP (cAMP) functions as the extracellular chemoattractant in the aggregation phase of *Dictyostelium* development. There is some question, however, concerning what role, if any, it plays intracellularly in motility and chemotaxis. To test for such a role, the behavior of null mutants of *acaA*, the adenylyl cyclase gene that encodes the enzyme responsible for cAMP synthesis during aggregation, was analyzed in buffer and in response to experimentally generated spatial and temporal gradients of extracellular cAMP. *acaA*$^-$ cells were defective in suppressing lateral pseudopods in response to a spatial gradient of cAMP and to an increasing temporal gradient of cAMP. *acaA*$^-$ cells were incapable of chemotaxis in natural waves of cAMP generated by majority control cells in mixed cultures. These results indicate that intracellular cAMP and, hence, adenylyl cyclase play an intracellular role in the chemotactic response. The behavioral defects of *acaA*$^-$ cells were surprisingly similar to those of cells of null mutants of *regA*, which encodes the intracellular phosphodiesterase that hydrolyzes cAMP and, hence, functions opposite adenylyl cyclase A (ACA). This result is consistent with the hypothesis that ACA and RegA are components of a receptor-regulated intracellular circuit that controls protein kinase A activity. In this model, the suppression of lateral pseudopods in the front of a natural wave depends on a complete circuit. Hence, deletion of any component of the circuit (i.e., RegA or ACA) would result in the same chemotactic defect.

When *Dictyostelium* amoebae deplete their environment of nutrients, they aggregate and then, as a multicellular unit, undergo morphogenesis to generate a sporangium composed of a stalk supporting a cap containing spores (11). During aggregation, cells both relay the chemoattractant cyclic AMP (cAMP) through the population as a series of outwardly moving, nondissipating waves (38) and respond to the information in the waves by surging in a pulsatile manner toward the original aggregation center (1, 48).

Pitt et al. (21) first identified and characterized the gene *acaA*, which encodes the adenylyl cyclase that produces the extracellular cAMP that serves as the chemotactic signal. Cells of the null mutant *acaA*$^-$ were incapable of aggregating because they could not release a chemotactic signal (21). Pitt et al. (21) found that if *acaA*$^-$ cells were induced to undergo early development by pulsing them experimentally with extracellular cAMP, they were then capable of undergoing chemotaxis in an experimentally generated spatial gradient of cAMP. Furthermore, *acaA*$^-$ cells artificially pulsed with cAMP made fruiting bodies, albeit smaller than those of wild-type cells. These observations were consistent with a purely extracellular role for cAMP in chemotaxis. However, it was subsequently demonstrated that the null mutant of the intracellular phosphodiesterase RegA and the null mutant of the protein kinase A (PKA) regulatory subunit were defective in their responses to an increasing temporal gradient of cAMP associated with the front of a natural wave and, therefore, were incapable of chemotaxis in natural cAMP waves generated by majority wild-type cells in mixtures (53, 55). Since RegA is responsible for the degradation of intracellular cAMP (24) and PKA is presumably regulated by intracellular cAMP (37), these results suggested that intracellular cAMP, synthesized primarily by the adenylyl cyclase encoded by *acaA* during aggregation, may play an intracellular role in the chemotactic response to the natural cAMP wave. This suggestion was further supported by observations of Wang and Kuspa (45) that overexpression of the gene that encodes the catalytic subunit of cAMP-dependent PKA in *acaA*$^-$ cells resulted in the formation of fruiting bodies in cell populations that had not been experimentally pulsed with the extracellular cAMP through early development, indicating that intracellular cAMP indeed controls PKA during early development. To test whether cAMP plays an intracellular as well as extracellular role in chemotaxis, we used computer-assisted two-dimensional (2D) and three-dimensional (3D) reconstruction and motion analysis methods (30, 31) to analyze, first, the basic motile behavior of *acaA*$^-$ cells in the absence of a cAMP signal and, second, responses to experimentally generated spatial and temporal gradients of cAMP (33). *acaA*$^-$ cells pulsed artificially with cAMP have been shown to express both pulse-independent genes, including those essential for chemotaxis, such as *carA*, which encodes the cAMP receptor (13, 35), *gpaB*, which encodes the Gα2 protein (22), and *pdsA*, which encodes the extracellular phosphodiesterase (17), as well as pulse-dependent genes (10). Our results indicate that adenylyl cyclase A plays a role in the suppression of lateral pseudopod formation in response to a

* Corresponding author. Mailing address: 302 BBE, Department of Biological Sciences, The University of Iowa, Iowa City, IA 52242. Phone: (319) 335-1117. Fax: (319) 335-2772. E-mail: david-soll@uiowa.edu.

positive spatial gradient of cAMP and to an increasing temporal gradient of cAMP, behaviors essential for normal chemotaxis in the natural cAMP wave (33). We also provide a logical explanation for the paradoxical observation that the defects in the chemotactic behavior of the deletion mutant of *acaA*$^-$, which encodes the cyclase that catalyzes cAMP formation, and of the deletion mutant of *regA*$^-$, which encodes the phosphodiesterase that hydrolyzes cAMP, are similar.

MATERIALS AND METHODS

Origin, maintenance, and development of strains. The *acaA*$^-$ mutant was generated in strain JH10 by targeted disruption of the *acaA* gene (21). An independent mutant of *acaA*, *acaA*$^-$(r), was obtained in a screen of strain AX4 cells mutagenized by using restriction enzyme-mediated integration (16). For experimental purposes, control and mutant cells obtained from frozen stocks were grown in HL-5 medium (3). Cells were grown in liquid medium in petri dishes since attachment under these conditions promoted a higher proportion of mononuclear cells. Cells were harvested at confluency.

To initiate development, cells were gently released from the dish bottom and washed in buffered salts solution (BSS; 20 mM KCl, 2.5 mM $MgCl_2$, 20 mM KH_2PO_4 [pH 6.40]) (36). Control cells were distributed on filter pads saturated with BSS at a cell density of 5×10^6 per cm^2 (29) and harvested at the onset of aggregation (approximately 6 h) (28), the stage at which wild-type cells achieve maximum velocity (42). Cells of the two mutant lines were pulsed in suspension every 6 min with 50 nM cAMP (46) over a 6-h period (see Results for an explanation of this method).

Behavioral analyses. To analyze basic motile behavior, harvested cells washed in BSS were distributed on the glass wall of a Sykes-Moore perfusion chamber (Bellco Glass, Vineland, N.J.) positioned on the stage of an upright microscope and perfused with buffer, as previously described (5, 46, 56). To analyze chemotactic behavior in a spatial gradient of cAMP, cells were dispersed on the bridge of either a Plexiglas chemotaxis chamber (40), designed after that of Zigmond (57), or a quartz chamber (26). BSS alone was added to one well and BSS plus 10^{-6} M cAMP was added to the other well bordering the bridge, according to methods previously described (26, 40). To analyze behavior in a sequence of temporal waves generated under conditions in which spatial gradients were not established, cells were challenged with four temporal waves of cAMP in sequence in a Sykes-Moore chamber according to methods previously described (41, 48). To analyze the response of cells to the rapid addition of cAMP, cells in a Sykes-Moore chamber were perfused first with BSS, then with BSS containing either 10^{-6} or 10^{-5} M cAMP according to methods previously described (50). To analyze mutant cell behavior in natural cAMP waves, *acaA*$^-$ cells were grown overnight in nutrient medium containing 5×10^{-5} M DiI (Molecular Probes, Eugene, Oreg.) for vital staining, washed in BSS, and mixed with unstained control cells at a ratio of 1 to 9, respectively, according to methods previously described (46, 55, 56). Cells were then distributed on a 35-mm-diameter petri dish and analyzed during the aggregation process by simultaneous transmitted and fluorescence microscopy through a laser scanning confocal microscope as previously described (46). Since the behavioral parameters under all experimental conditions of JH10 cells, which were the control for *acaA*$^-$ cells, and AX4 cells, which were the control for *acaA*$^-$(r) cells, were highly similar, we have only presented the data for JH10 cells.

Reconstruction and analysis with the 2D- and 3D-DIAS programs. The methods for computer-assisted 2D reconstruction and quantitative motion analysis were similar to those previously described (30, 31, 32). Only cells translocating at average velocities of ≥3.0 μm per min over a 10-min period were motion analyzed. This proportion was greater than 70% for every cell preparation analyzed. Methods for the four-dimensional reconstruction of migrating cells have been described elsewhere in detail (7, 32, 52).

F-actin staining. F-actin was stained with Oregon green-conjugated phalloidin (Molecular Probes, Inc.) according to methods recently described in detail (46). Cells were visualized with a Bio-Rad Radiance 2100MP laser scanning confocal microscope at 0.2-μm increments in the *z* axis. Both projection images through the entire stack of optical sections and single optical sections 1 μm above the substratum are presented for each analyzed cell.

TABLE 1. 2D-DIAS analysis of basic motile behavior when perfused with BSS in the absence of chemoattractant[a]

Parameter	Value for strain		P[b]
	JH10	*acaA*$^-$	
Motility parameters			
No. of cells	20	33	
Instantaneous velocity (μm/min)	7.8 ± 2.8	8.3 ± 3.2	NS
Directional persistence	0.36 ± 0.20	0.37 ± 0.19	NS
Directional change (°)	48 ± 16	41 ± 12	NS
Positive flow (%/5 s)	9.4 ± 2.7	9.8 ± 2.4	NS
Negative flow (%/5 s)	9.0 ± 2.6	9.2 ± 2.1	NS
Shape parameters			
No. of cells	20	33	
Maximum width (μm)	9.8 ± 2.0	10.2 ± 2.0	NS
Maximum length (μm)	22.5 ± 4.5	18.2 ± 3.5	1×10^{-3}
Roundness (%)	47 ± 16	64 ± 8	1.4×10^{-4}
Mean convexity (°)	653 ± 130	531 ± 91	8.9×10^{-4}
Mean concavity (°)	294 ± 131	171 ± 91	9.2×10^{-4}
Radial deviation (%)	37 ± 8	28 ± 4	1.9×10^{-4}

[a] Parameters (means ± standard deviations) are calculated according to the method of Soll (30).
[b] P values of ≥0.05 were considered nonsignificant (NS).

RESULTS

Developmental regulation of cell motility. Previously, we demonstrated that at the onset of aggregation, *Dictyostelium* amoebae exhibit an increase in velocity, which is assessed by removing cells from developing cultures and measuring velocity in a chamber in which cells are perfused with BSS (42). We have used the developmentally regulated increase in velocity as a developmental landmark for comparing mutant and parental strains (5, 29, 42, 46, 55, 56). Control JH10 cells exhibited a velocity peak after 6 h on development pads that was similar to that reported for strain AX3 (42) and strain AX2 (49). The instantaneous velocity of JH10 cells increased from 3.5 ± 1.0 μm per min at 0 h to 7.7 ± 1.8 μm per min at 6 h, the onset of aggregation, and then decreased upon further development. For the mutant *acaA*$^-$, several pulsing regimes were tested. We found that pulsing both *acaA*$^-$ and *acaA*$^-$(r) cells in suspension cultures every 6 min with 50 nM cAMP over a 6-h period resulted in increases in velocity that paralleled that of control cells on development pads. The instantaneous velocity of pulsed *acaA*$^-$ cells increased from 4.2 ± 0.8 μm per min at 0 h to 9.0 ± 2.0 μm per min at 6 h and then decreased with further pulsing. Similar results were obtained for *acaA*$^-$(r) cells. Both control JH10 and AX4 cells pulsed in a similar fashion exhibited a less distinct velocity peak. We therefore compared mutant cells, *acaA*$^-$ and *acaA*$^-$(r), pulsed with cAMP for 6 h in suspension with control cells developed for 6 h on pads, conditions that produced the most reproducible, optimal, and comparable motility and shape data in the two strains.

Basic motile behavior. *acaA* cells translocated in buffer at mean instantaneous velocities statistically indistinguishable from that of aggregation-competent control JH10 cells (Table 1). They also exhibited mean directional persistence and mean directional change parameters similar to those of JH10 cells (Table 1). Finally, the mean positive and negative flow measures, motility parameters computed independently of the cell centroid (30), were also statistically indistinguishable between *acaA*$^-$ and control JH10 cells (Table 1). Perimeter tracks of control cells (Fig. 1A) and mutant cells (Fig. 1B) were similar in length and number of sharp turns, reflecting the similarity in motility parameters.

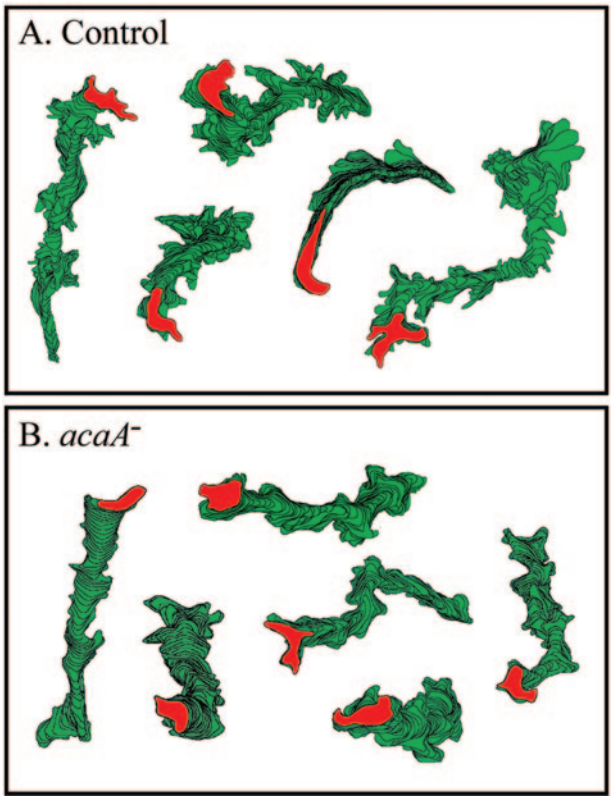

FIG. 1. Perimeter tracks revealed no difference in the behaviors of representative control (JH10) (A) and mutant cells (B) translocating in buffer. The red reconstruction represents the last in each track. Cells were reconstructed at 8-sec intervals.

However, shape parameters differed. *acaA*$^-$ cells were on average less elongate than control cells. This was reflected in computed shape parameters (Table 1). For instance, while the roundness parameter for control cells was 47 ± 16, that for *acaA*$^-$ cells was 64 ± 8 (Table 1). A 2D-DIAS analysis of *acaA*$^-$(r) cells migrating in buffer revealed a behavior profile similar to AX4 control cells. Again, although the velocity and directional change parameters of *acaA*$^-$(r) and control AX4 cells were similar, the shape parameters suggest that *acaA*$^-$(r) cells were rounder. For instance, the roundness parameter of AX4 cells was 43.4 ± 10.4 (number of cells [*n*] = 48), while that of *acaA*$^-$(r) cells was 71 ± 6 ($n = 20$).

The similarity between control and mutant cells in directionality parameters (Table 1) and the similarity in persistence reflected in perimeter tracks (Fig. 1) suggested that the average frequency of turning and, hence, the average frequency of lateral pseudopod formation (51) of control and mutant cells migrating in buffer were similar. Measurements of the frequency of lateral pseudopod formation compared over a 10-min period demonstrated that this was indeed the case for both *acaA*$^-$ and *acaA*$^-$(r) (Table 2). Together, these results support the conclusion that in the absence of adenylyl cyclase A, the basic motile behavior of a cell is normal, although there is an alteration in shape.

Behavior in a spatial gradient of cAMP. In contrast to migration in buffer, the behavior of control and mutant cells differed markedly in a spatial gradient of cAMP. Cells of the two mutant lines translocated at lower mean instantaneous velocities than control cells, with lower mean directional persistence and higher mean directional change values (Table 3). Although mutant cell lines exhibited positive chemotaxis, both the chemotactic index and the proportion of the population exhibiting a positive chemotactic index were significantly reduced when compared to that of control cells (Table 3). A histogram of chemotactic indices revealed that while the majority of control cells exhibited chemotactic indices between +0.61 and +1.00, the majority of mutant cells exhibited chemotactic indices between −0.20 and +0.80 (Fig. 2A). Therefore, although mutant cells were able to assess and make net progress up a spatial gradient of cAMP, the responses were highly inefficient. This was obvious in comparisons of perimeter tracks of control JH10 cells (Fig. 2B) and *acaA*$^-$ cells (Fig. 2C). Cells turned more often, suggesting a defect in the suppression of lateral pseudopod formation. Measurements revealed that *acaA*$^-$ and *acaA*$^-$(r) cells in spatial gradients of cAMP formed lateral pseudopods at seven and eight times, respectively, the frequency of control JH10 cells (Table 2). While control JH10 cells in a cAMP gradient exhibited an eightfold reduction in the frequency of lateral pseudopod formation from that in buffer, both *acaA*$^-$ and *acaA*$^-$(r) cells exhibited no reduction (Table 2). These results demonstrate that although mutant cells are chemotactically responsive to a spatial gradient of cAMP, they are not able to suppress lateral pseudopod formation when oriented in a gradient, as control cells are able to do (44), resulting in abnormal turns that reduce the efficiency of chemotaxis.

As was the case in buffer, the shape parameters measured in a spatial gradient of cAMP indicated that mutant cells were less elongate than control cells in spatial gradients of cAMP (Table 3). To obtain a more complete picture of aberrant shape and pseudopod formation, a representative control JH10 cell and a representative *acaA*$^-$ cell undergoing chemotaxis in a spatial gradient of cAMP were reconstructed in 3D by using 3D-DIAS software (7, 31, 32, 52), as shown in Fig. 3A and B, respectively. While the representative control cell was elongate and extended a single dominant anterior pseudopod in the direction of increasing cAMP (Fig. 3A), the mutant cell

TABLE 2. Frequency of lateral pseudopod formation in buffer, in spatial gradients of cAMP, and in the front of simulated temporal waves of cAMP

Cell type	Frequency of lateral pseudopod formation per 10 min[a]		
	In buffer	In spatial gradient of cAMP	In front of temporal wave (10^{-8} to 10^{-6} M)
JH10	5.1 ± 2.7 (13)	0.6 ± 1.2 (11)	1.1 ± 2.1 (19)
acaA$^-$	4.6 ± 2.4 (27)	4.2 ± 1.7 (26)	3.1 ± 3.0 (29)
acaA$^-$ (r)	4.7 ± 1.2 (23)	4.9 ± 2.7 (17)	2.8 ± 3.7 (20)

[a] The method for assessing pseudopod frequency can be found in Wessels et al. (47). Frequencies are provided as means ± standard deviations. Individual cells (total numbers of cells examined are given in parentheses) were analyzed for 10-min periods. *P* values were computed by a Student's *t* test; a *P* value of $>5 \times 10^{-2}$ was considered nonsignificant. *P* values for the comparison of JH10 cells with *acaA*$^-$ and *acaA*$^-$ (r) cells were nonsignificant in buffer; in spatial gradient, the *P* values were 6×10^{-8} and 2×10^{-6}, respectively, and in front of the temporal wave, they were 4×10^{-6} and 2×10^{-3}, respectively. In buffer versus spatial gradient, the *P* values were 4×10^{-5} for JH10 cells and nonsignificant for *acaA*$^-$ and *acaA*$^-$ (r) cells. In buffer versus the front of the temporal wave, the *P* values were 1×10^{-4} for JH10 cells, 1×10^{-2} for *acaA*$^-$ cells, and 6×10^{-2} for *acaA*$^-$ (r) cells.

TABLE 3. 2D-DIAS analysis of chemotaxis in a spatial gradient of cAMP[a]

Parameter	Value for strain			P[b]	
	JH10	*acaA*$^-$	*acaA*$^-$ (r)	*acaA*$^-$ vs JH10	*acaA*$^-$ (r) vs JH10
Motility and chemotaxis parameters					
No. of cells	20	26	16		
Instantaneous velocity (μm/min)	11.2 ± 3.9	6.8 ± 3.0	6.8 ± 1.8	2.3×10^{-4}	1.5×10^{-4}
Directional persistence	0.82 ± 0.14	0.44 ± 0.21	0.31 ± 0.16	3.0×10^{-9}	3.6×10^{-11}
Directional change (°/4 s)	16 ± 5	30 ± 10	46 ± 9	1.5×10^{-7}	2.6×10^{-11}
Chemotactic index	+0.80 ± 0.18	+0.15 ± 0.35	+0.11 ± 0.30	2.1×10^{-13}	2.3×10^{-13}
Percent positive chemotaxis	100	65	63	5.8×10^{-10}	3.1×10^{-8}
Shape parameters					
No. of cells	20	26	16		
Maximum width (μm)	6.2 ± 0.8	9.9 ± 1.6	9.9 ± 2.7	9.1×10^{-13}	6.4×10^{-5}
Maximum length (μm)	22.3 ± 5.0	17.8 ± 3.7	16.1 ± 3.3	1.8×10^{-3}	8.0×10^{-5}
Roundness (%)	45 ± 9	63 ± 11	66 ± 7	1.3×10^{-7}	4.5×10^{-9}
Radial deviation (%)	43 ± 5	28 ± 5	26 ± 4	2.1×10^{-13}	2.3×10^{-13}

[a] Parameters (means ± standard deviations) are calculated according to the method of Soll (30).
[b] P values of ≥0.05 were considered nonsignificant.

was rounder, had greater height, and extended a less compact, apparently fragmented anterior pseudopod and multiple lateral pseudopods, on average smaller than the dominant pseudopod of the control cell (Fig. 3B). The 3D reconstructions of additional *acaA*$^-$ and *acaA*$^-$(r) cells and additional control cells confirmed differences.

Responses to temporal gradients of cAMP. During natural aggregation, *Dictyostelium* amoeba response to the temporal as well as spatial gradients associated with the different phases of the wave (33, 41, 43, 44, 48). A cell suppresses lateral pseudopod formation and translocates in a rapid and persistent fashion (i.e., surges) in response to the increasing temporal gradient of cAMP in the front of the wave. As extracellular cAMP approaches peak concentration, the cell stops forming new pseudopods, becomes less elongate, and begins to retract its dominant anterior pseudopod. This results in a sharp decrease in velocity. In response to the decreasing temporal gradient in the back of a wave, a cell remains less elongate but reinitiates pseudopod formation. The new pseudopods are comparatively small and extend in all directions. In the back of the wave, a cell makes no net progress in any one direction. This sequence of behavioral responses to the temporal components of a wave can be tested by challenging cells with four temporal waves of cAMP (10^{-8} M at the peak and 10^{-6} M at the trough) generated in a round perfusion chamber in which spatial gradients are not established (33, 41, 43, 48).

Control JH10 cells exhibited velocity peaks in the front of the last three in a series of four temporal waves of cAMP generated in the concentration range estimated for the natural wave ($<10^{-8}$ M at the trough and 10^{-6} M at the peak) (38) (Table 4), as previously described for JH10, AX3, and AX4 cells (41, 55, 56). The proportions of control cells exhibiting velocity surges in the front of waves 2, 3, and 4 were 68, 63, and 79%, respectively (Table 4). Cells of both mutants exhibited surges in the front of the last three in a series of four temporal waves of cAMP, but the surges occurred less consistently than those of control JH10 cells (Table 4). When the concentration range between the trough and peak of each of the four simulated waves of cAMP was increased by one order of magnitude (to 10^{-7} M at the trough and 10^{-5} M at the peak), the proportions of *acaA*$^-$ cells undergoing velocity surges increased to that of control cells (Table 4). Increasing the concentration range had no further effect on the proportion of control cells surging in the front of temporal waves (Table 4). Examples of the velocity surges exhibited by control and *acaA*$^-$ cells in the fronts of waves 2, 3, and 4 are presented in Fig. 4A and B, respectively.

Since mutant cells were defective in suppressing lateral pseudopod formation in a spatial gradient of cAMP, we tested whether they were also defective in a front of simulated temporal wave. In the front of a temporal wave with troughs and peaks of 10^{-8} and 10^{-6} M cAMP, respectively, control cells formed lateral pseudopods at a frequency equivalent to 1.1 ± 2.1 per 10 min, which is a fivefold decrease from that in buffer (Table 2). In marked contrast, cells of the two mutant lines formed lateral pseudopods in the front of a temporal wave at frequencies of 3.1 ± 3.0 and 2.8 ± 3.7 per 10 min, respectively, representing less than a onefold decrease in each case (Table 2). These frequencies were threefold higher than the frequency of control cells in the front of a temporal wave (Table 2). When the concentration range of simulated temporal waves was increased one order of magnitude from 10^{-7} M at the trough and 10^{-5} M at the peak, there was no further effect on the frequency of lateral pseudopod formation in control cells (1.1 ± 2.1 [n = 19] per 10 min in the normal range and 1.2 ± 2.4 [n = 11] per 10 min in the increased range), and only a small effect on *acaA*$^-$ cells (3.1 ± 3.0 [n = 29] per 10 min in the normal range and 2.6 ± 2.4 [n = 15] in the latter range). These results indicate that *acaA*$^-$ cells are defective in suppressing lateral pseudopod formation in response not only to an increasing spatial gradient of cAMP but also to an increasing temporal gradient of cAMP.

To test whether *acaA*$^-$ cells underwent the normal shape changes associated with the different phases of a wave, difference pictures were generated of representative control JH10 and *acaA*$^-$ cells responding to the third in a series of four simulated temporal waves of cAMP in the concentration range of 10^{-7} to 10^{-5} M cAMP. Control cells underwent the normal changes in shape associated with the peak and back of a wave (6, 33). They were elongate with a dominant anterior pseudo-

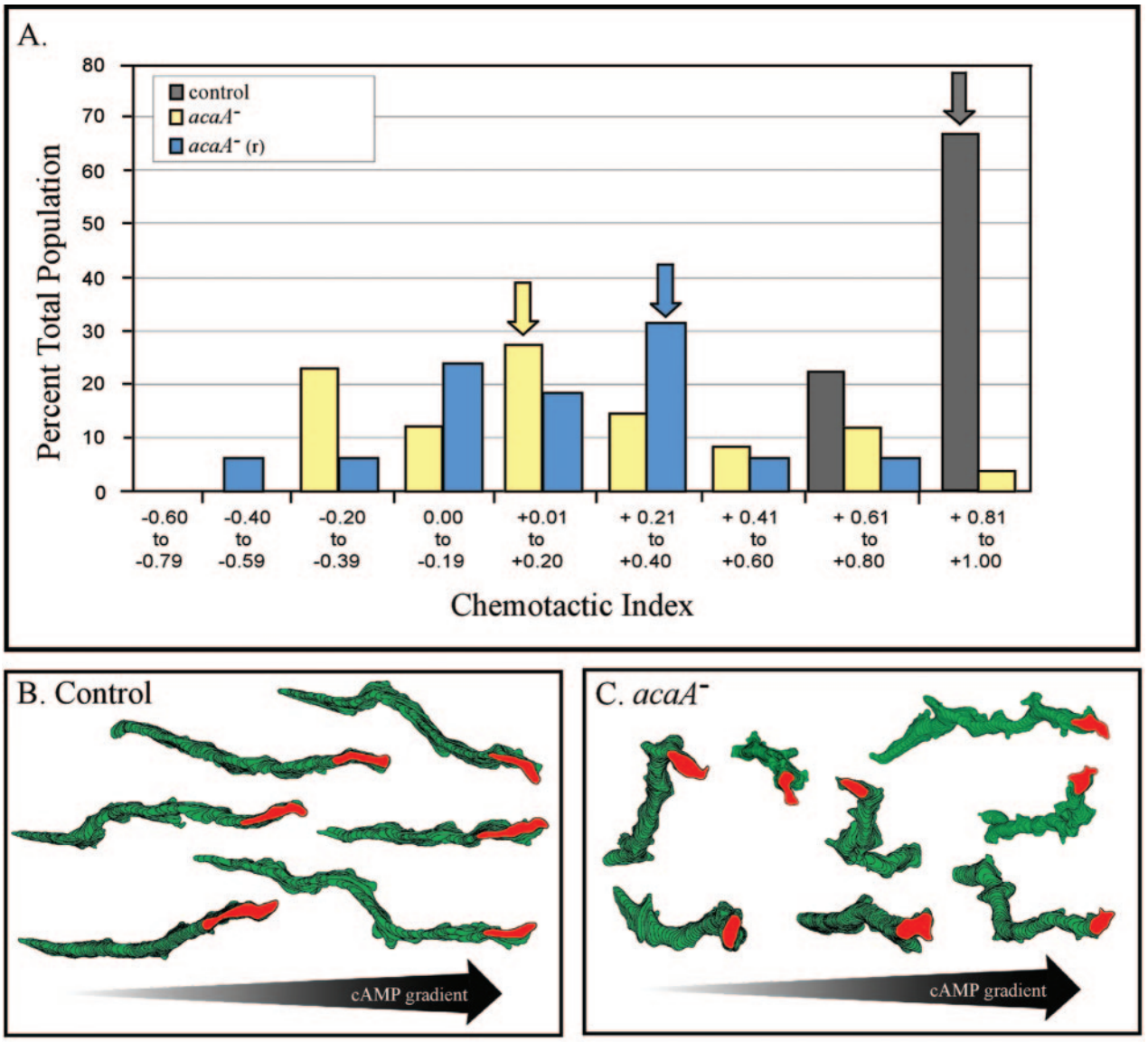

FIG. 2. *acaA*$^-$ and *acaA*$^-$(r) cells are chemotactically responsive to a spatial gradient of cAMP but exhibit a decrease in efficiency. (A) Histograms of the chemotactic indices of individual control (JH10) and mutant [*acaA*$^-$ and *acaA*$^-$(r)] cells reveal a decrease in the efficiency of mutant cell chemotaxis. Arrows indicate the mean chemotactic index for each cell line. Over 20 individual cells were analyzed for each cell line. Note that the majority of chemotactic indices of the two mutant lines were in the positive range, but the distributions were at far lower chemotactic values than JH10 cells. (B and C) Perimeter tracks reveal that although net progress is on average in the direction of the increasing spatial gradient of cAMP, mutant cells turn more often, taking cells off track. The red reconstruction represents the last in each track. Cells were reconstructed at 8-sec intervals.

pod (green expansion zone) in the front of the wave (Fig. 4C), became less elongate and partially retracted their anterior pseudopod at the peak of the wave (Fig. 4D), and remained relatively apolar in the back of the wave (Fig. 4E). As in buffer and in a spatial gradient of cAMP, mutant cells, although polar, were less elongate than control cells in the front of the wave due to increased lateral pseudopod formation (Fig. 4F). At the peak of the wave, mutant cells rounded up (Fig. 4G) like control cells (Fig. 4D), and in the back of the wave, mutant cells remained less polar (Fig. 4H), like control cells (Fig. 4E). Similar results were obtained with *acaA*$^-$(r) cells (data not shown). These results demonstrate that while *acaA*$^-$ cells are defective in suppressing lateral pseudopod formation in response to the increasing temporal gradient of cAMP in the front of a wave, they respond normally to the peak and decreasing temporal gradient of cAMP in the back of a wave.

Response to the rapid addition of cAMP. A second method for analyzing the response of cells to the high concentration of cAMP attained at the peak of a natural wave is to add 10^{-6} M cAMP rapidly to cells crawling in buffer in a perfusion chamber, so that the concentration of cAMP rises from 0 M to 10^{-6} M in approximately 12 seconds (33, 50). When control cells were treated with cAMP in this manner, there was a 56% reduction in average instantaneous velocity (Table 5). When

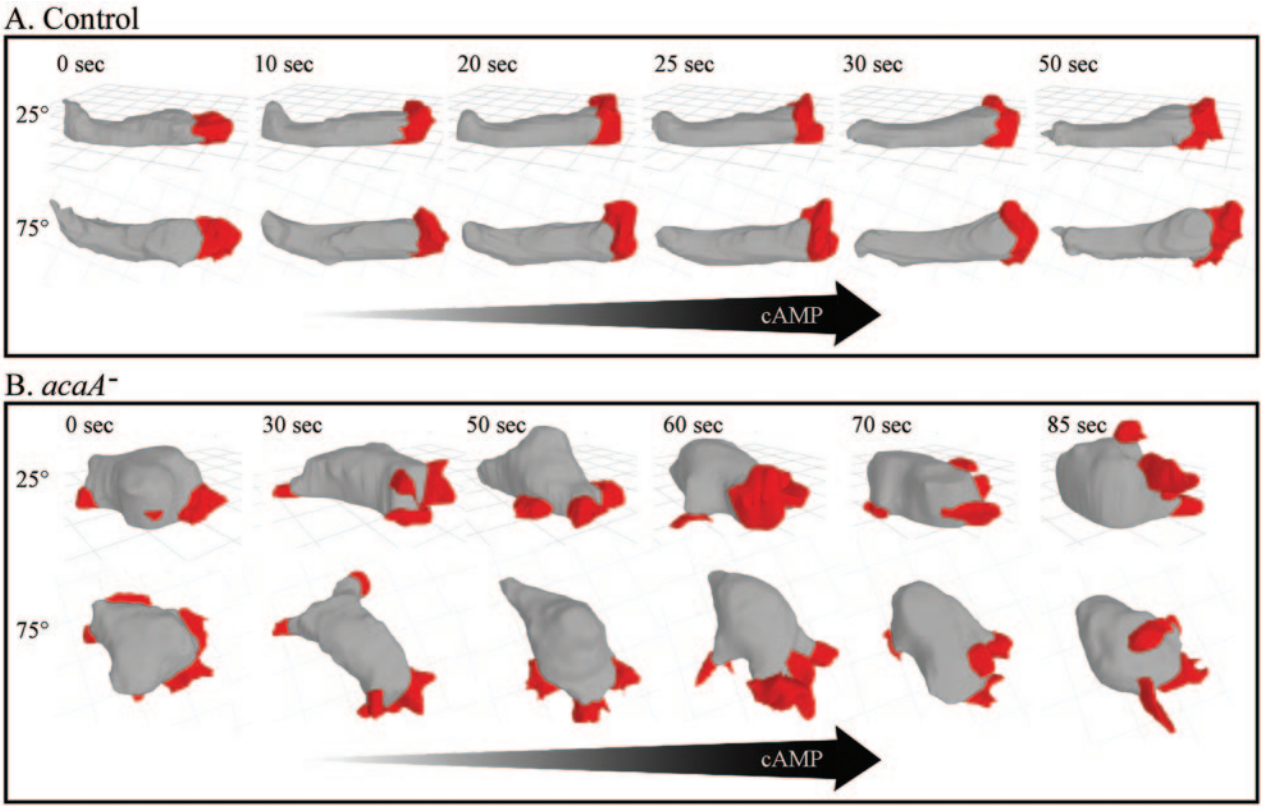

FIG. 3. 3D-DIAS reconstructions of a representative control (JH10) cell (A) and a representative *acaA*$^-$ cell (B) translocating up a spatial gradient of cAMP reveal abnormalities both in pseudopod formation and cell shape. Cell bodies are colored gray and pseudopodia are red. Each cell was viewed at 25 and 75° angles. The arrows indicate the direction of the increasing spatial gradient of cAMP. Note the elongate shape and single dominant anterior pseudopod of the control cell, distinct from the round, more hemispheric shape and complex multipseudopodial extensions of the mutant cell.

acaA$^-$ and *acaA*$^-$(r) cells were treated in this manner, there was a 26 and 21% reduction, respectively (Table 5). When 10^{-5} M cAMP was rapidly added, the percent decrease in instantaneous velocity of *acaA*$^-$ cells was similar to that of control cells (Table 5). This is demonstrated in velocity plots before and after addition of 10^{-5} M cAMP for a representative JH10 cell (Fig. 5A) and a representative *acaA*$^-$ cell (Fig. 5B).

Chemotaxis in a natural wave of cAMP. To test whether *acaA*$^-$ cells responded to natural waves of cAMP, they were stained with the membrane dye DiI and mixed with unstained control cells at a ratio of 1 to 9, respectively (46). The cell mixture was then incubated under conditions that supported natural aggregation. Under these conditions, mutant cells were exposed to waves of cAMP relayed by the majority control cells in a natural aggregation territory. During the aggregation process in mixed cultures, cells were simultaneously monitored by phase microscopy, which imaged all cells (mutant and control) in a field, and laser scanning confocal microscopy, which distinguished the minority of vitally stained mutant cells. Two different fields of view are presented in Fig. 6 in each of which one representative control JH10 cell (black) and one neighboring *acaA*$^-$ cell (red) have been monitored over time.

The control JH10 cells exhibited velocity surges at average intervals of approximately 8 min over the 70-min period of analysis (Fig. 6A and C). The net direction of control cells was towards the aggregation center (Fig. 6B and D). *acaA*$^-$ cells also exhibited velocity surges, but these surges were more erratic than those of control cells. While some of the surges were synchronized with those of neighboring control cells, others were out of sync or missed. For each of eight independently analyzed *acaA*$^-$ cells, the net direction appeared random, indicating that in spite of their capacity to surge in response to the front of sequential cAMP waves, *acaA*$^-$ cells made little net progress towards an aggregation center, in contrast to neighboring control cells.

TABLE 4. *acaA*$^-$ cells surge in velocity in response to the increasing phases of simulated temporal waves of cAMP

Cell type	No. of cells	Concn of cAMP (M)		% of cells exhibiting velocity surge in front of:		
		Peak	Trough	Wave 2	Wave 3	Wave 4
Control JH10	19	10^{-6}	10^{-8}	68	63	79
acaA$^-$	38	10^{-6}	10^{-8}	29	42	68
acaA$^-$ (r)	28	10^{-6}	10^{-8}	49	39	64
Control JH10	11	10^{-5}	10^{-7}	73	55	82
acaA$^-$	16	10^{-5}	10^{-7}	75	63	75
Control JH10[a]	20	0	0	5	5	0

[a] In this control, JH10 cells were analyzed while continually being perfused with buffer lacking chemoattractant and analyzed during time periods comparable to the fronts of temporal waves.

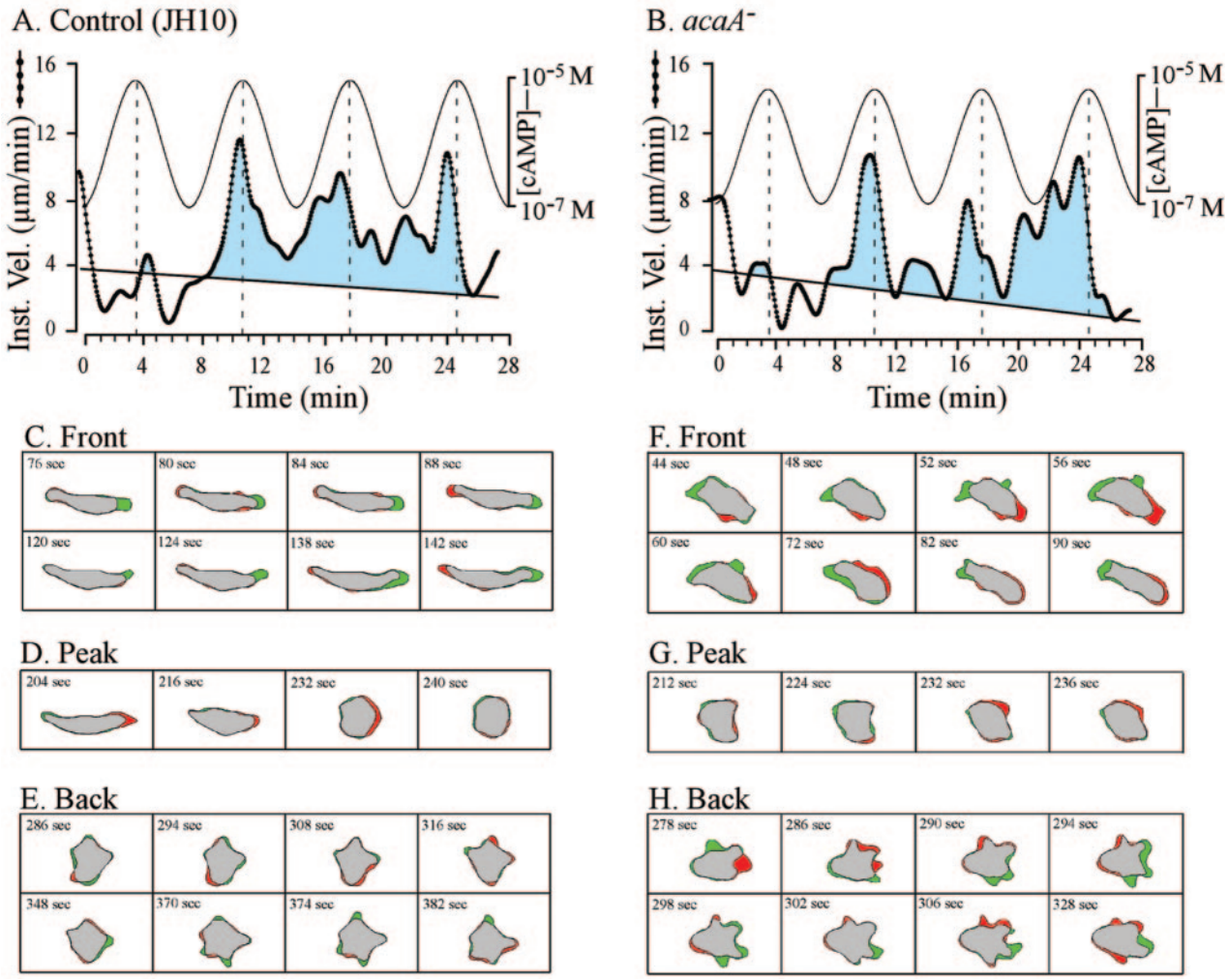

FIG. 4. The velocity of a representative control (JH10) cell (A) and a representative *acaA*$^-$ cell (B) in a series of four simulated temporal waves of cAMP generated in a perfusion chamber reveals no difference in the surging responses to the front of the three last in a series of four simulated temporal waves of cAMP. Difference pictures of a representative control (JH10) cell (C, D, and E) and a representative *acaA*$^-$ cell (F, G, and H) reveal normal behavioral responses to the peak and back of the third in a series of four temporal waves of cAMP. In this case, the peak concentration was 10^{-5} M and the trough concentration was 10^{-7} M for each simulated temporal wave in order to obtain a maximum response in *acaA*$^-$ cells (see text). In panels A and B, the instantaneous velocity of each cell is plotted as a function of time. The estimated waves of cAMP are diagrammed at the top of each plot. Velocity above an arbitrary threshold line drawn from 4 to 2 μm is shown in blue to accentuate the time of velocity surges in response to the second, third, and fourth waves. In the difference pictures in panels C through H, expansion zones are shown in green and contraction zones are shown in red. Note the differences in the front of the wave between the control (C) and *acaA*$^-$ (F) for cell shape and lateral pseudopod formation.

F-actin reorganization in temporal waves. F-actin localization in *Dictyostelium* is modulated by the temporal dynamics of the cAMP wave in a manner that may require myosin heavy chain II dephosphorylation (8). In order to determine if intracellular adenylyl cyclase was a component of this pathway, F-actin was stained in control and *acaA*$^-$ cells migrating in buffer as well as in cells experiencing an increasing temporal cAMP gradient. In control JH10 cells migrating in buffer, F-actin stained primarily in pseudopodial projections, with faint staining in the cortex and cytoplasm (Fig. 7A and B), as previously described (46, 55). In the front of a simulated temporal wave of cAMP, F-actin also stained most intensely in pseudopodial projections, but there was a marked increase in cortical staining (Fig. 7C and D), as previously described (46, 55). Mutant *acaA*$^-$ cells migrating in buffer exhibited a staining pattern (Fig. 7E and F) similar to that of JH10 cells in buffer (Fig. 7A and B), and *acaA*$^-$ cells responding to the front of a temporal wave exhibited an increase in cortical staining (Fig. 7G and H), similar to that of control JH10 cells (Fig. 7C and D).

DISCUSSION

In *Dictyostelium*, the chemotactic signal is in the form of an outwardly moving, nondissipating wave of cAMP (38). Studies of null mutants of *acaA* had led to the perception that the role of cAMP was primarily extracellular (23). However, there were several indirect observations suggesting that cAMP might also

TABLE 5. *acaA*$^-$ cells respond to a rapid increase in cAMP by a reduction in velocity but require a higher concentration of cAMP than control cells for a normal response[a]

cAMP concn	Cell type	No. of cells	Instantaneous velocity before addition (μm/min)	Instantaneous velocity after addition (μm/min)	% Decrease in instantaneous velocity
10^{-6} M	JH10	9	7.2 ± 1.2	3.1 ± 1.2	56
	acaA$^-$	19	7.2 ± 1.9	5.3 ± 1.6	26
	acaA$^-$ (r)	7	7.7 ± 1.8	6.0 ± 1.3	21
10^{-5} M	JH10	4	6.2 ± 0.8	3.2 ± 0.4	49
	acaA$^-$	5	8.8 ± 2.9	4.7 ± 1.1	45

[a] Cells were first perfused for 5 min with buffered salts solution alone in a round perfusion chamber. Perfusion solution was then switched to buffered salts solution plus chemoattractant at the concentration indicated. The velocities were averaged for each individual cell over a 5-min period before addition of chemoattractant and a 5-min period after its addition.

play a role as an intracellular signal in the chemotactic response. First, null mutants of *regA*$^-$, which encodes an intracellular phosphodiesterase believed to hydrolyze intracellular cAMP (24, 37), were defective in suppressing lateral pseudopod formation in response to increasing spatial and increasing temporal gradients of cAMP; hence, *regA*$^-$ cells were unable to undergo normal chemotaxis in response to natural waves of cAMP (53). Second, a mutant of the regulatory subunit of cAMP-regulated PKA, which rendered the catalytic subunit constitutively active, was defective in cell shape and chemotaxis (55). Third, overexpression of the gene encoding the catalytic subunit of PKA in *acaA*$^-$ cells led to fruiting body formation, the final stage in the developmental program beginning with aggregation, implicating intracellular cAMP in the normal regulation of PKA (45). Together, these observations suggested that cAMP may also play an intracellular role in the regulation of the chemotactic response. Presumably, its effect would be mediated through the regulation of PKA, which in turn would regulate one or more proteins involved in the chemotactic response. This has been demonstrated to be the case in nerve growth cone guidance in *Xenopus* embryos in which intracellular cAMP modulates $Ca2^+$ entry into nerve growth cones (34) in a signal transduction pathway essential for turning and chemotaxis in response to the extracellular signal netrin-1 (19).

The two independent *acaA* null mutants, *acaA*$^-$ and *acaA*$^-$(r), exhibited positive chemotaxis in spatial gradients of cAMP, but the response in both cases was highly inefficient. The chemotactic indices of the two mutant strains were +0.15 and +0.11, respectively, compared to +0.80 for control cells. These responses could be considered marginal, or questionable, if it were not for the fact that the proportion of cells that exhibited a chemotactic response for the two mutant strains was 65 and 63%, respectively. It was clear from the perimeter tracks that *acaA*$^-$ cells could orient in a spatial gradient of cAMP but when on track could not suppress lateral pseudopod formation and turning. This was evident in direct measures of the frequency of lateral pseudopod formation. Varnum-Finney et al. (44) documented that cells adjust direction in a spatial gradient of cAMP through lateral pseudopod formation and turning. As a cell becomes more on track (i.e., more aligned with the spatial gradient), it decreases proportionately the frequency of lateral pseudopod formation and turning (44). Cells lacking adenylyl cyclase A were, therefore, defective in suppression. This was also true in response to an increasing temporal gradient of cAMP. The behavioral phenotype of the double mutant *acaA*$^-$*acrA*$^-$, which also lacks an adenylyl cyclase not implicated in aggregation (27), was similar to that of the *acaA*$^-$ mutants analyzed here (data not shown).

The increasing temporal gradient of cAMP associated with the front of a natural wave causes an increase in velocity and suppression of lateral pseudopod formation (33, 43, 48). In *acaA*$^-$ cells, it caused the former but not the latter. Since this common behavioral defect of *acaA*$^-$ cells was exhibited in experimentally generated spatial and temporal gradients of

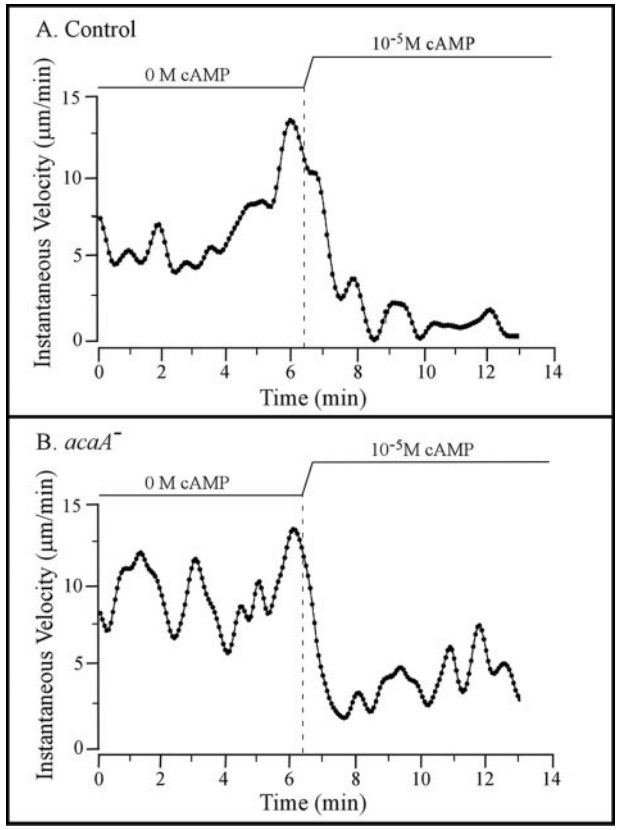

FIG. 5. *acaA*$^-$ cells undergo a normal reduction in velocity in response to the rapid addition of 10^{-5} M cAMP. The concentration of 10^{-5} M rather than 10^{-6} M was used to obtain a maximum response in *acaA*$^-$ cells (see text). Cells were perfused with buffer in a perfusion chamber for 6 min and then treated with buffer plus 10^{-5} M cAMP for seven additional minutes.

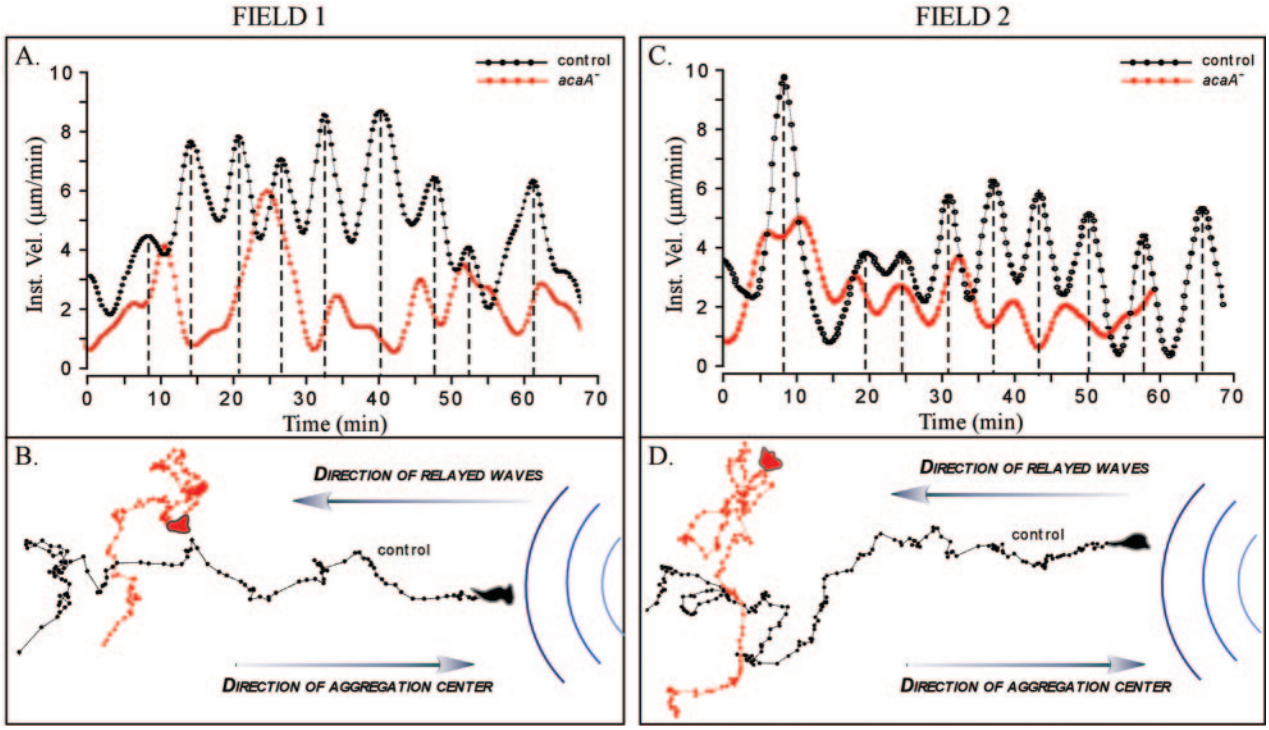

FIG. 6. *acaA*$^-$ cells do not respond normally to natural waves of cAMP relayed through an aggregation territory of predominantly control (JH10) cells in a mixture of mutant and control cells in a ratio of one to nine, respectively. *acaA*$^-$ cells (red) were vitally stained with DiI. Control cells (black) were unstained. (A and C) Instantaneous velocity of control (JH10) and *acaA*$^-$ cells, in close proximity in two different aggregation fields, responding to sequential waves of cAMP in natural aggregation territories. (B and D) Centroid tracks of the control (JH10) and *acaA*$^-$ cell responding to sequential waves of cAMP relayed through the fields in the respective aggregation territories. The instantaneous velocity plots of control and mutant cells were smoothed with Tukey windows of 5, 15, 60, 15, and 5. Note that the velocity surges of *acaA*$^-$ cells occurred but were more erratic than those of the control cells in close proximity (A and C) and that *acaA*$^-$ cells made no net progress towards the aggregation center, the source of the natural waves (B and D).

cAMP, it cannot be attributed to the absence of an extracellular signal. Rather, it can only be attributed to the absence of adenylyl cyclase and the intracellular cAMP it is responsible for synthesizing. Furthermore, the observation that the frequency of lateral pseudopod extension in *regA*$^-$ and *acaA*$^-$ cells is normal during basic motile behavior, but is not suppressed under gradient conditions, sets these mutants apart from another class of mutants that includes the sphingosine-1 phosphate lyase null mutants (15), *myoA*$^-$ (5), *myoB*$^-$ (5), and *chc*$^-$ (49). In contrast to *regA*$^-$ and *acaA*$^-$, mutants in this latter group also abnormally extend multiple lateral pseudopods during basic motile behavior in buffer. Taken together, these data support the conclusion that the inability to suppress lateral pseudopods in *acaA*$^-$ and *regA*$^-$ cells is specific to the cAMP response rather than a broader or more generalized deregulation of lateral pseudopod extension.

It has been proposed that in waves of cAMP relayed through natural aggregation territories, the positive spatial gradient of cAMP in the front of the wave orients a cell in the direction of an aggregation center, and the positive temporal gradient of cAMP associated with the front of the wave stimulates translocation and suppression of lateral pseudopod formation (33). The defects of *acaA*$^-$ cells in both spatial and temporal gradients of cAMP generated in vitro should affect their capacity to undergo chemotaxis in a natural wave of cAMP. Mixing experiments demonstrated this was indeed the case.

TABLE 6. Comparison of the behavioral phenotypes of mutants *acaA*$^-$ and *regA*$^-$ in buffer and in response to chemotactic signals

Behavioral parameter	Phenotype	
	acaA$^-$	*regA*$^-$
In buffer		
Frequency of lateral pseudopod formation	Normal	Normal
Instantaneous velocity	Normal	Normal
Frequency of turning	Normal	Normal
In spatial gradient cAMP		
Suppression of lateral pseudopod formation	Defective	Defective
Instantaneous velocity	Normal	Normal
Frequency of turning	Defective	Defective
Chemotactic index	Defective	Defective
In temporal gradienct cAMP[a]		
Suppression of lateral pseudopod formation (FW)	Defective	Defective
Velocity surge (FW)	Normal	Normal
Frequency of turning (FW)	Defective	Defective
Cortical relocalization of F-actin (FW)[b]	Normal	Normal
Loss of elongate morphology (PW)	Normal	Normal
Multiple pseudopod formation (BW)	Normal	Normal
Chemotaxis in natural wave of cAMP	Defective	Defective

[a] FW, front of temporal wave; PW, peak of temporal wave; BW, back of temporal wave.

[b] Data for *regA*$^-$ behavior are from Wessels et al. (53); data for cortical relocalization of F-actin are from K. Daniels, D. Wessels, and D. R. Soll (unpublished observations).

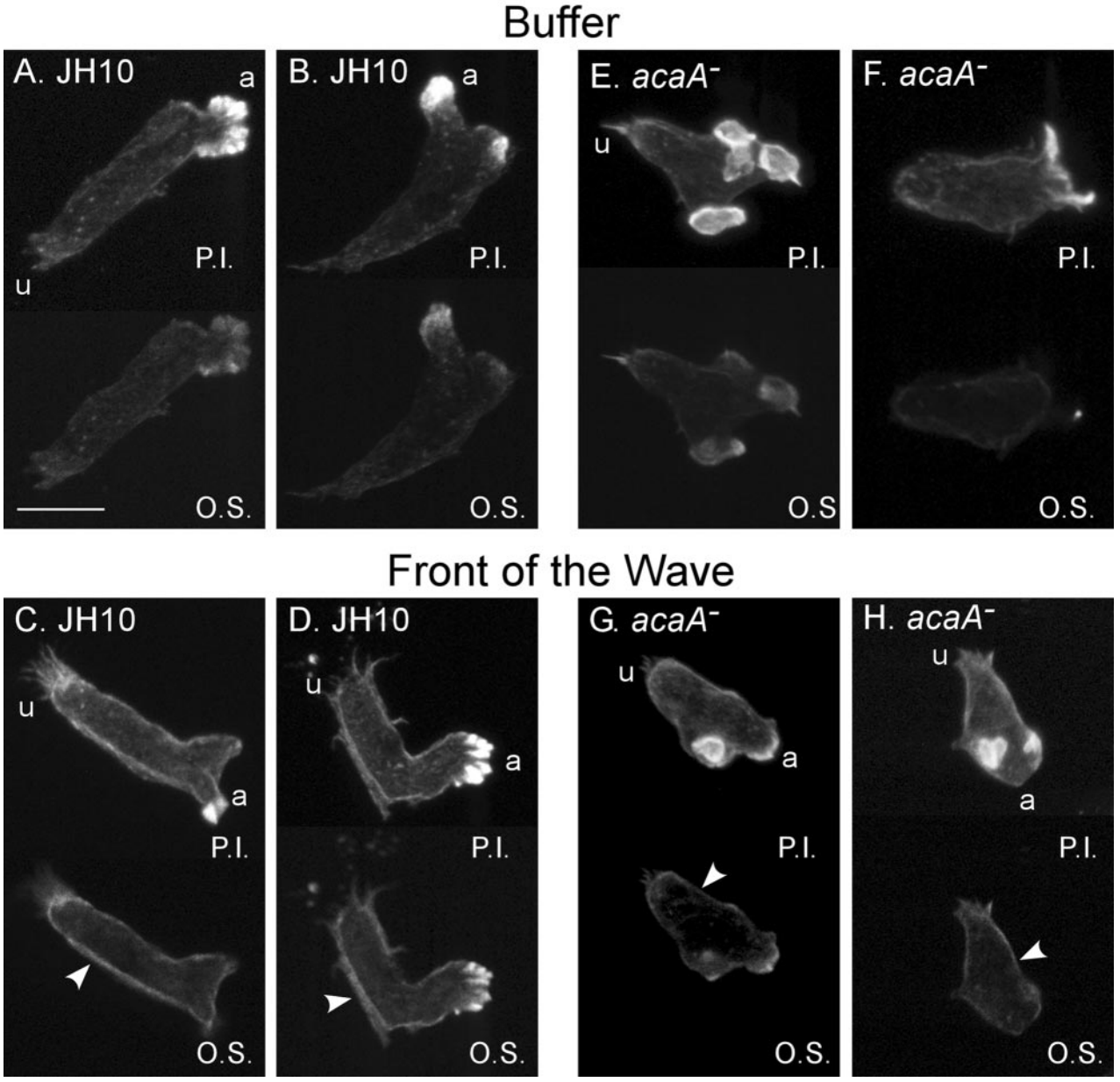

FIG. 7. The staining patterns of F-actin reveal normal cortical localization in *acaA*$^-$ cells in response to the front of the wave. Control (JH10) and *acaA*$^-$ cells were stained with Oregon green-phalloidin in buffer and in the front of the third in a series of four temporal waves of cAMP. Cells were analyzed by laser scanning confocal microscopy. a, anterior end of cell; u, uropod; P.I., projection image of the entire stack of optical sections from laser scanning confocal microscopy; O.S., optical section 1 μm above the substratum. The increase in cortical staining is noted in optical sections by arrowheads in panels C, D, G, and H. Scale bar, 5 μm.

The specific chemotactic defects of *acaA*$^-$ cells are likely to result from the reduced levels of intracellular cAMP. The resulting attenuation of PKA activity may directly affect cytoskeletal processes or may act indirectly through alterations in the pattern of gene expression during early development. However, microarray-based studies have shown that the early genes expressed during the period preceding the time when the chemotactic defects were observed (time, 6 h) are normally expressed in *acaA*$^-$ cells given exogenous pulses of cAMP (10). While it is impossible to rule out misexpression of a critical gene that was not surveyed in the microarray experiments, there is no reason to suspect such a defect in the mutant cells. It is also possible that there are consequences to the loss of adenylyl cyclase A other than synthesis of cAMP. *Dictyostelium* cells have the highly conserved CAP protein that binds both adenylyl cyclase and G-actin which may play a role in organizing the cytoskeleton (9, 14). However, the distribution of F-actin in cells migrating in buffer and the redistribution of F-actin to the cortex in response to an increasing temporal gradient of cAMP in the front of a wave were found to be indistinguishable in wild-type and *acaA*$^-$ cells. The similarity between the chemotactic defects exhibited by the *regA*$^-$ mu-

tant and the *acaA*$^-$ mutant, both of which affect cAMP levels, makes it most likely that the chemotactic defects result from alterations in the intracellular cAMP signal.

Paradoxically, the null mutant of *acaA*, which encodes the adenylyl cyclase A responsible for synthesizing cAMP in response to the dynamics of receptor occupancy (2, 20, 21, 23,27), and the null mutant of *regA*, which encodes the phosphodiesterase responsible for breaking down that signal intracellularly (25), exhibit similar chemotactic defects (53) (Table 6). While both mutants behave normally in the absence of a chemotactic signal, neither can suppress lateral pseudopod formation in a normal fashion in increasing spatial or temporal gradients of cAMP. Hence, neither mutant can undergo chemotaxis in natural waves of cAMP generated by majority control cells in mixing experiments. Resolution of this apparent paradox may be found in the hypothesized regulatory circuit emanating from the cAMP receptor, which includes CAR1, ERK2, adenylyl cyclase A, RegA, and PKA (18). It has been proposed that this circuit is oscillatory and regulates the cyclic increases in cAMP both intracellularly and extracellularly (18). Deletion of any one of the major components of the circuit would destroy the circuit and the resulting intracellular oscillations of cAMP. If the chemotactic behaviors that were found to be commonly defective in the *acaA*$^-$ and *regA*$^-$ mutants depend upon an intact, oscillating circuit (18), it would explain why deletion of either of these genes, with opposite functions, results in a similar behavioral defect. A similar result has been obtained for the phosphodiesterase mutant *dunce* and the cyclase mutant *rutabaga* in *Drosophila melanogaster*. Both result in loss of memory (4, 39) and both exhibit similar depressed rates of growth cone motility (12, 54).

ACKNOWLEDGMENTS

This research was supported by National Institutes of Health grants HD-18577 to D.R.S. and GM60447 and GM62350 to W.F.L.

The authors are indebted to P. Devreotes for sharing mutants.

REFERENCES

1. **Alcantara, F., and M. Monk.** 1974. Signal propagation during aggregation in the slime mould *Dictyostelium discoideum*. J. Gen. Microbiol. **85:**321–334.
2. **Anjard, C., F. Söderborn, and W. F. Loomis.** 2001. Requirements for the adenylyl cyclases in the development of *Dictyostelium*. Development **128:** 3649–3654.
3. **Cocucci, S., and M. Sussman.** 1970. RNA in cytoplasmic and nuclear fractions of cellular slime mold amebas. J. Cell Biol. **45:**399–407.
4. **Dudai, Y.** 1988. Neurogenic dissection of learning and short-term memory in *Drosophila*. Annu. Rev. Neurosci. **11:**537–563.
5. **Falk, D. L., D. Wessels, L. Jenkins, T. Pham, S. Kuhl, M. A. Titus, and D. R. Soll.** 2003. Shared, unique and redundant functions of three myosin Is (MyoA, MyoB and MyoF) in motility and chemotaxis in *Dictyostelium*. J. Cell. Science **116:**3985–3999.
6. **Geiger, J., D. Wessels, and D. R. Soll.** 2003. Human PMNs respond to temporal waves of chemoattractant like *Dictyostelium*. Cell Motil. Cytoskeleton **56:**27–44.
7. **Heid, P., E. Voss, and D. R. Soll.** 2002. 3D-DIASemb: a computer-assisted system for reconstructing and motion analyzing in 4D every cell and nucleus in a developing embryo. Develop. Biol. **245:**329–347.
8. **Heid, P., D. Wessels, K. Daniels, P. Gibson, H. Zhang, E. Voss, and D. R. Soll.** 2004. The role of myosin heavy chain phosphorylation in *Dictyostelium* motility, chemotaxis and F-actin localization. J. Cell Sci. **117:**4819–4835.
9. **Hubbersteg, A. V., and E. P. Motillo.** 2002. Cyclase associated proteins: CAPacity for linking signal transduction and actin polymerization. FASEB J. **490:**487–499.
10. **Iranfar, N., D. Fuller, and W. F. Loomis.** 2003. Genome-wide expression analyses of gene regulation during early development of *Dictyostelium discoideum*. Eukaryot. Cell **2:**664–670.
11. **Kessin, R. H.** 2001. *Dictyostelium*: evolution, cell biology, and the development of multicellularity. Cambridge University Press, Cambridge, United Kingdom.
12. **Kim, Y. T., and C.-F. Wu.** 1996. Reduced growth cone motility in cultured neurons from *Drosophila* memory mutants with a defective cyclic AMP cascade. J. Neruosci. **16:**5593–5602.
13. **Klein, P., T. Sun, C. Saxe, A. Kimmel, R. Johnson, and P. Devreotes.** 1988. A chemoattractant receptor controls development in *Dictyostelium discoideum*. Science **241:**1467–1472.
14. **Ksiazek, D., H. Brandstetter, L. Israel, G. Bourenkov, G. Katchalova, L. Janssen, H. Bartunik, A. Noegel, M. Schleicher, and T. Holak.** 2003. Structure of the N-terminal domain of adenylyl cyclase-associated protein (CAP) from *Dictyostelium discoideum*. Structure **11:**1171–1178.
15. **Kumar, A., D. Wessels, K. Daniels, H. Alexander, S. Alexander, and D. R. Soll.** 2004. Sphingosine-1 phosphate plays a role in the suppression of lateral pseudopod formation during *Dictyostelium discoideum* cell migration and chemotaxis. Cell Motil. Cytoskeleton **59:**227–241.
16. **Kuspa, A., and W. F. Loomis.** 1992. Tagging developmental genes in *Dictyostelium* by restriction enzyme-mediated integration of plasmid DNA. Proc. Natl. Acad. Sci. USA **89:**8803–8807.
17. **Lacombe, M., G. Podgorski, J. Franke, and R. Kessin.** 1986. Molecular cloning and developmental expression of the cyclic nucleotide phosphodiesterase gene of *Dictyostelium discoideum*. J. Biol. Chem. **261:**16811–16817.
18. **Maeda, M., S. Lu, G. Shaulsky, Y. Miyazaki, H. Kuwayama, Y. Tanaka, A. Kuspa, and W. F. Loomis.** 2004. Periodic signaling controlled by an oscillatory circuit that includes protein kinases ERK2 and PKA. Science **304:**875–878.
19. **Nishiyama, M., A. Hoshino, L. Tsai, J. Henley, Y. Goshima, M. Tessier-Lavigne, M. Poo, and K. Hong.** 2003. cAMP/cGMP-dependent modulation of Ca2+ channels sets the polarity of nerve growth-cone turning. Nature **423:**990–995.
20. **Pitt, G. S., R. Brandt, K. C. Lin, P. N. Devreotes, and P. Schaap.** 1993. Extracellular cAMP is sufficient to restore developmental gene expression and morphogenesis in *Dictyostelium* cells lacking the aggregation adenylyl cyclase (ACA). Genes Dev. **7:**2172–2180.
21. **Pitt, G. S., N. Milona, J. Borleis, K. C. Lin, R. R. Reed, and P. N. Devreotes.** 1992. Structurally distinct and stage-specific adenylyl cyclase genes play different roles in *Dictyostelium* development. Cell **69:**305–315.
22. **Pupillo, M., A. Kumagai, G. Pitt, R. Firtel, and P. N. Devreotes.** 1989. Multiple α subunits of guanine nucleotide-binding proteins in *Dictyostelium*. Proc. Natl. Acad. Sci. USA **86:**4892–4896.
23. **Saran, S., M. E. Meima, E. Alvarez-Curto, K. E. Weening, D. E. Rozen, and P. Schaap.** 2002. cAMP signaling in *Dictyostelium*. J. Musc. Res. Cell Motil. **23:**793–802.
24. **Shaulsky, G., R. Escalante, and W. F. Loomis.** 1996. Developmental signal transduction pathways uncovered by genetic suppressors. Proc. Natl. Acad. Sci. USA **93:**15260–15265.
25. **Shaulsky, G., D. Fuller, and W. F. Loomis.** 1998. A cAMP-phosphodiesterase controls PKA-dependent differentiation. Development **125:**691–699.
26. **Shutt, D. C., L. M. Jenkins, E. Carolan, J. Stapleton, K. Daniels, R. Kennedy, and D. R. Soll.** 1998. T cell syncytia induced by HIV release T cell chemoattractants: demonstration with a newly developed single cell chemotaxis chamber. J. Cell Sci. **111:**99–109.
27. **Söderbom, F., C. Anjard, N. Iranfar, D. Fuller, and W. F. Loomis.** 1999. An adenylyl cyclase that functions during late development of *Dictyostelium*. Development **126:**5463–5471.
28. **Soll, D. R.** 1979. Timers in developing systems. Science **203:**841–849.
29. **Soll, D. R.** 1987. Methods for manipulating and investigating developmental timing in *Dictyostelium discoideum*, p. 413–431. *In* J. Spudich (ed.), Methods in cell biology, vol. 28. Academic Press, Inc., New York, N.Y.
30. **Soll, D. R.** 1995. The use of computers in understanding how animal cells crawl. Int. Rev. Cytol. **163:**43–104.
31. **Soll, D. R., and E. Voss.** 1998. Two and three dimensional computer systems for analyzing how cells crawl, p. 25–52. *In* D. R. Soll and D. Wessels (ed.), Motion analysis of living cells. Wiley-Liss, Inc., New York, N.Y.
32. **Soll, D. R., E. Voss, O. Johnson, and D. J. Wessels.** 2000. Three-dimensional reconstruction and motion analysis of living crawling cells. Scanning **22:**249–257.
33. **Soll, D. R., D. Wessels, H. Zhang, and P. Heid.** 2003. A contextual framework for interpreting the roles of proteins in motility and chemotaxis in *Dictyostelium discoideum*. J. Musc. Res. Cell Motil. **23:**659–672.
34. **Song, H.-J., and M.-M. Poo.** 1999. Signal transduction underlying growth cone guidance by diffusible factors. Curr. Opin. Neurobiol. **9:**355–363.
35. **Sun, T. J., and P. N. Devreotes.** 1991. Gene targeting of the aggregation state cAMP receptor cAR1 in *Dictyostelium*. Genes Dev. **5:**572–582.
36. **Sussman, M.** 1987. Cultivation and synchronous morphogenesis of *Dictyostelium* under controlled experimental conditions. Methods Cell Biol. **28:**9–29.
37. **Thomason, P. A., D. Traynor, G. Cavet, W. T. Chang, A. Harwood, and R. Kay.** 1998. An intersection of the cAMP/PKA and two component signal transduction system in *Dictyostelium*. EMBO J. **17:**2838–2845.
38. **Tomchik, K. J., and P. N. Devreotes.** 1981. Adenosine 3′ 5′-monophosphate waves in *Dictyostelium discoideum*: a demonstration by isotope dilution-fluorography technique. Science **212:**443–446.

39. **Tully, T., and W. G. Quinn.** 1985. Classical conditioning and retention in normal and mutant *Drosophila melanogaster*. J. Comp. Physiol. **157:**263–277.
40. **Varnum, B., and D. R. Soll.** 1984. Effect of cAMP on single cell motility in *Dictyostelium*. J. Cell Biol. **99:**1151–1155.
41. **Varnum, B., K. Edwards, K., and D. R. Soll.** 1985. *Dictyostelium* amoebae alter motility differently in response to increasing versus decreasing temporal gradients of cAMP. J. Cell Biol. **101:**1–5.
42. **Varnum, B., K. Edwards, and D. R. Soll.** 1986. The developmental regulation of single cell motility in *Dictyostelium discoideum*. Devel. Biol. **113:**218–227.
43. **Varnum-Finney, B., K. Edwards, E. Voss, and D. R. Soll.** 1987. Amoebae of *Dictyostelium discoideum* respond to an increasing temporal gradient of the chemoattractant cAMP with a reduced frequency of turning: evidence for a temporal mechanism in amoeboid chemotaxis. Cell Motil. Cytoskeleton **8:**7–17.
44. **Varnum-Finney, B., E. Voss, and D. R. Soll.** 1987. Frequency and orientation of pseudopod formation of *Dictyostelium discoideum* amoebae chemotaxing in a spatial gradient: further evidence for a temporal mechanism. Cell Motil. Cytoskeleton **8:**18–26.
45. **Wang, B., and A. Kuspa.** 1997. *Dictyostelium* development in the absence of cAMP. Science **277:**251–254.
46. **Wessels, D., R. Brincks, S. Kuhl, V. Stepanovic, K. J. Daniels, G. Weeks, C. J. Lim, D. Fuller, W. F. Loomis, and D. R. Soll.** 2004. RasC plays a selective role in the transduction of temporal gradient information in the cAMP wave of *Dictyostelium*. Eukaryot. Cell **3:**646–662.
47. **Wessels, D., J. Murray, G. Jung, J. Hammer, and D. R. Soll.** 1991. Myosin IB null mutant of *Dictyostelium* exhibits abnormalities in motility. Cell Motil. Cytoskeleton **20:**301–315.
48. **Wessels, D., J. Murray, and D. R. Soll.** 1992. Behavior of *Dictyostelium* amoebae is regulated primarily by the temporal dynamics of the natural cAMP wave. Cell Motil. Cytoskeleton **23:**145–156.
49. **Wessels, D., J. Reynolds, O. Johnson, E. Voss, R. Burns, K. Daniels, E. Garrard, T. O'Hallaran, and D. R. Soll.** 2000. Clathrin plays a novel role in the regulation of cell polarity, pseudopod formation, uropod stability and motility in *Dictyostelium*. J. Cell Sci. **113:**26–36.
50. **Wessels, D., N. Schroeder, E. Voss, A. Hall, J. Condeelis, and D. R. Soll.** 1989. cAMP mediated inhibition of intracellular particle movement and actin reorganization in *Dictyostelium*. J. Cell Biol. **109:**2841–2851.
51. **Wessels, D., H. Vawter-Hugart, J. Murray, and D. R. Soll.** 1994. Three dimensional dynamics of pseudopod formation and the regulation of turning during the motility cycle of *Dictyostelium*. Cell Motil. Cytoskeleton **27:**1–12.
52. **Wessels, D., E. Voss, N. Von Bergen, R. Burns, J. Stites, and D. R. Soll.** 1998. A computer-assisted system for reconstructing and interpreting the dynamic three-dimensional relationships of the outer surface, nucleus and pseudopods of crawling cells. Cell Motil. Cytoskeleton **41:**225–246.
53. **Wessels, D., H. Zhang, J. Reynolds, K. Daniels, P. Heid, S. Liu, A. Kuspa, G. Shaulsky, W. F. Loomis, and D. R. Soll.** 2000. The internal phosphodiesterase RegA is essential for the suppression of lateral pseudopods during *Dictyostelium* chemotaxis. Mol. Biol. Cell **11:**2803–2820.
54. **Wu, C.-F.** 1998. Neuronal growth cone motility: contributions from neurogenetic analyses of cultural *Drosophila* neurons, p. 235–262. *In* D. R. Soll and D. Wessels (ed.), Motion analysis of living cells. Wiley-Liss, Inc., New York, N.Y.
55. **Zhang, H., P. Heid, D. Wessels, K. Daniels, T. Pham, W. F. Loomis, and D. R. Soll.** 2003. Constitutively active protein kinase A disrupts motility and chemotaxis in *Dictyostelium discoideum*. Eukaryot. Cell. **2:**62–75.
56. **Zhang, H., D. Wessels, P. Fey, K. Daniels, R. Chisholm, and D. R. Soll.** 2002. Phosphorylation of the myosin regulatory light chain plays a role in cell motility and polarity during *Dictyostelium* chemotaxis. J. Cell Sci. **115:**1733–1747.
57. **Zigmond, S. H.** 1977. The ability of polymorphonuclear leukocytes to orient in gradients of chemotactic factors. J. Cell Biol. **75:**606–616.